



ISSN 2314-5609
Nuclear Sciences Scientific Journal
5, 91-108
2016

<http://www.ssnma.com>

PETROGRAPHY, GAMMA RADIATION MEASUREMENTS AND DOSE RATE, NORTHEASTERN UMARA AREA, SOUTH EASTERN DESERT, EGYPT

NASSER M. MOGHAZY

Nuclear Materials Authority, Cairo, Egypt

ABSTRACT

The northern part of Um Ara alkali feldspar microgranite has subjected to extensive post-magmatic metasomatic reworking resulting in development of amazonitized and albitized zones, reflecting K- and Na metasomatism leading to gross enrichment in U and Th towards the more evolved phases (e.g., albitized zones). Spectrometric survey data indicate that eU in Dokhan volcanics has the range of 2 to 42 ppm with an average value of 10 ppm and in monzogranites. It varies from 3 to 13 ppm with an average of 7 ppm while in alkali feldspar microgranites eU contents vary from 3 to 282 ppm with an average value of 30 ppm. The (eTh) contents in Dokhan volcanics ranges from 5-51 ppm with an average 18 ppm, in monzogranites their content was in the range of 11 to 47 ppm with an average value of 27 ppm where it ranges from 14 to 83 ppm with an average 46 ppm in alkali feldspar granite. The enhanced uranium content in altered zones was attributed to disseminated and fracture filling uranophane, autonite, in addition to other U and Th bearing minerals (such as columbite, zircon, monazite, xenotime and fluorite). Gamma-radiation dose rate and annual effective dose equivalents in mSv/y, Radium equivalent activity, external (H_{ex}) and internal hazard index (H_{in}) and gamma activity index (I_γ) for all investigated samples were calculated to assess the potential radiation hazard for people living in dwellings made of the studied granites. Alkali feldspar granite activities would suggest that caution must be taken when using granites as building materials because they have radioactivity above the proposed acceptable level.

INTRODUCTION

The Egyptian younger granites are a good target for uranium exploration in the Eastern Desert of Egypt belonging to the third epoch of uranium mineralization (0.70-0.50 Ga) during the upper Proterozoic-Cambrian times (Tilsley, 1979; Dahlkamp 1979, 1980; Tones, 1981; Nash et al., 1981). Um Ara granites have $^{206}\text{Pb}/^{238}\text{U}$ crystallization age of 603 ± 14 Ma of zircons separated from the alkali feldspar microgranites (Moussa et al., 2008). Uranium mineralization related to granitic intrusions can be genetically divided into two groups: primary and secondary uranium deposits (Jiashu and Zehong, 1982). The first

is fixed in the rocks during the crystallization of magma, while the second is precipitated by various geological processes later from dissolved and transported uranium comes from primary uranium. Secondary uranium can be divided into three types; (1) absorbed uranium in altered minerals such as montmorillonite, chlorite and limonite; (2) interstitial uranium at the grain boundaries which formed as a result of hydrothermal solution migration along the interstices of minerals in granites, and (3) uranium in microfractures, the formation of this type is due to the circulation of hydrothermal solution. The secondary uranium mineralization in Um Ara alkali

feldspar microgranite formed at a two stage of metallogenic model as proposed by (Abd El-Naby, 2009); the first stage was dominated by hydrothermal alteration accompanied by albitization, K-feldspathization, desilicification, chloritization etc.. The second stage occurred near-surface profile where circulating meteoric water played an important role in mobilizing the early formed U-bearing minerals.

Several uranium deposits of the vein-, and disseminated-types occur at the peripheries of some granitic plutons in the Egyptian basement of the Eastern Desert [e.g., Gabal Gattar (Salman et al., 1990; Roz, 1994; Abu Zeid, 1995; Shalaby, 1996), Gabal El Misikat, (Bakhit, 1978; Hussein, 1987; Abu Dief, 1985, 1992) Gabal El-Erediya (El Kasas, 1974), Gabal Um Ara (Abdel-Meguid, 1986; Ibrahim, 1986; Abdalla, 1996; Abdel-Meguid et al., 2007; Moussa et al., 2008; Abd El-Naby, 2009 and Gabal El-Sella (Ibrahim et al., 2005)]. The mineralogy of these occurrences is dominated by secondary uranium minerals and fluorite. The uranium mineralizations in these areas are structurally controlled and are commonly accompanied with hydrothermal alterations such as kaolinitization, argillization, carbonatization, ferrugination, silicification, microclintization, albitization and greisenization. It was also recognized that the development of late-magmatic to post-magmatic volatile-rich fluids played important role during the course of extraction, transportation and deposition of the rare metal assemblage in the Um Ara alkali feldspar granite (Abdalla, 1996).

The mineralogical composition of uranium deposits is dominated by uraninite and uranophane (Abdel-Meguid, 1986; Ibrahim, 1986) in Um Ara granite which is attributed to syngenetic and hydrothermal origin, while accessories are represented by zircon, apatite, fluorite, sphene, topaz and monazite. Uranium can be easily oxidized as U^{6+} in near-surface environment and is insoluble in the U^{4+} state forming soluble uranyl complex ion

$(UO_2)^{2+}$ that play the most important role in the U migration, leaching and weathering of granitic rocks may provide the source of the secondary U deposits.

The uranium exploration in the Um Ara area was first done by Sadek (1978), using a regional aeroradiometric survey which was followed by ground prospecting with portable γ -ray spectrometer conducted by Abdel Meguid (1986) and Ibrahim (1986). The Egyptian Nuclear Materials Authority was carried out an exploration program in Um Ara area to evaluate U deposits and to follow the radioactive mineralizations until 2000, (Mansour et al., 2000).

Some laboratory extraction studies using the heap-leaching technique on technological samples from Um Ara were carried out by Ibrahim (1994), Sayed (1996) and Awadallah (1999). They revealed that about 10-30% of the U content of the mineralized rock is found in refractory minerals.

The aim of the present study is to study the geology, petrographical characteristics of the altered alkali feldspar granite and radiological risks associated with the presence of radionuclides in Um Ara area. For this purpose radiation doses of gamma radiation were measured along spectrometric survey using portable RS-230 BGO gamma ray spectrometer for K%, eU, eTh and exposure dose rate (D) for the northeastern part of Um Ara pluton near the contact with Um Dobr dokhan volcanics.

GEOLOGIC SETTING

Um Ara area is located between lat. $22^{\circ} 36' - 22^{\circ} 39'$ and long. $33^{\circ} 47' - 33^{\circ} 52'$ about 230 km SE Aswan city close to the Sudanese border. The geology of Um Ara area was studied in detailed by many authors, e.g. (Abdel meguid, 1968; Ibrahim, 1986 and Abdalla, 1996). The study area comprises different types of igneous and metamorphic rocks of Precambrian-Early Paleozoic age. The basement complex sequence in this area are represented by melange rocks, metavol-

canics, Dokhan volcanics and granitic rocks (Fig. 1A, B). The melange rocks are represented by pelitic matrix of deep water sediments containing fragments of variable sizes of basalts, gabbros and serpentinites. The metavolcanics comprises lower mafic and upper felsic volcanics. The lower sequence comprises metapyroclastics, metabasalts and metadolerites, while metadacites represent the upper sequence. The Dokhan volcanics of G. Um Dobr are fresh felsic volcanics comprises banded flows and tuffs that range in composition from andesitic to rhyolitic. The whole basement sequence in the area is intruded by granitoid rocks represented by monzogranite pluton (589 Ma.) and alkali feldspar microgranite stock (556 Ma.). The time span between the emplacement of monzogranite and the alkali feldspar microgranite stock is about 33Ma., (K-Ar age of mica separates), (Abdalla, 1996 and Moussa, 2008). These granitic masses belong to the post-orogenic younger

granite magmatic activity (El Shazly, 1964), intruded the Egyptian Shield between 620-530 Ma. The monzogranite is an oval-shaped pluton trending NNE-SSE. It has homogeneous pinkish coarse-grained equigranular texture. The monzogranite is composed of microcline and microcline perthite, plagioclase, quartz and biotite. Scarce flakes of muscovite are also observed; titanite and magnetite are common accessory components.

The alkali feldspar microgranite is located at the northern and eastern part of Um Ara area as elongated belt trending NW-SE trend. It sends apophyses and offshots into the northern Dokhan volcanics of G. Um Dobr.

SAMPLING AND EXPERIMENTAL TECHNIQUES

Twenty five thin and polished sections representing all varieties of altered phases of alkali feldspar microgranites are prepared to

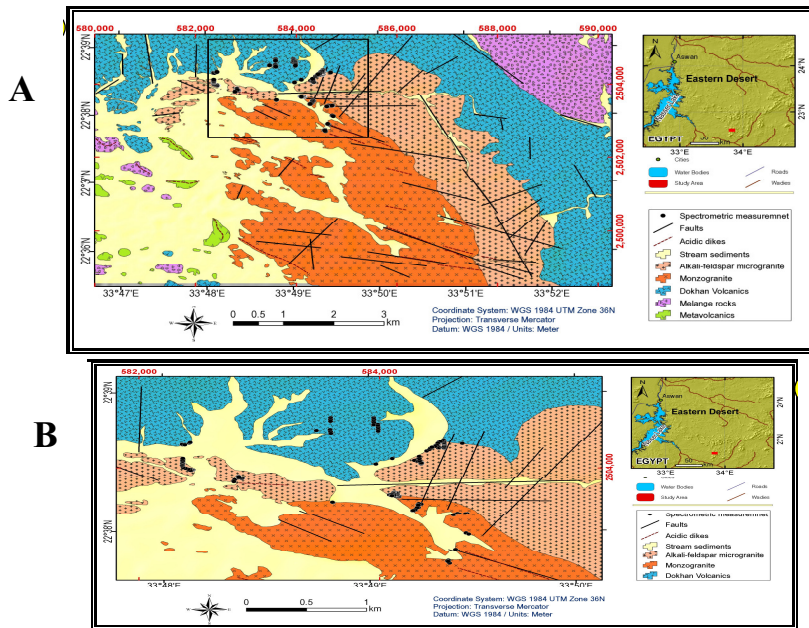


Fig. 1: (A) location and geological map of Um Ara area, (Modified after Abdalla, 1996) (B) The northeastern part of Um Ara area (the present study)

detect the textural variations and the mineralogical characteristics of alteration facies. The northeastern part of Um Ara area has been subjected to detailed field spectrometric investigations to detect radioelements concentrations and to measure the dose rate using the RS-230 BGO Super-Spec portable radiation detector, handheld unit spectrometer survey meter with high accuracy and its probable measurement errors was about 5%. The new RS-230 Spectrometer is the state-of-the-art in portable hand-held radiation spectrometer survey instrument for the Geophysical industry. It offers an integrated design with full weather protection, large detector, ease of use and the highest sensitivity in the market segment. This detector is full assay capability with data in K%, U (ppm), and Th (ppm), no radioactive sources required for proper operation. This procedure enables the use of the spectrometer to make qualitative determinations of U, Th and K compositions of all granitic phases.

Also, twenty two samples of altered alkali feldspar microgranites were chosen for analysing U-chemically (Uch) in the laboratory to compare their results with that of equivalent uranium contents (eU) of the same samples measured in the field to establish the equilibrium state.

PETROGRAPHICAL CHARACTERISTICS OF ALTERED ALKALI FELDSPAR MICROGRANITES

The petrographical study aims to delineate the relation between hydrothermal alterations and uranium potentiality in alkali feldspar microgranite. It is a fine-grained (< 2 mm), composed mainly of microcline, micropertite, albite, Quartz, biotite and minor white mica. Accessory minerals are columbite, zircon, xenotime, thorite, monazite and disseminated uranophane. Violet and colorless fluorite veinlets are locally abundant. Pegmatite veins are common and composed of coarse amazonite crystals (> 2 cm)

and quartz. The alkali feldspar granite was subjected to extensive late-magmatic metasomatism e.g, amazonitization and albitization granite which will be discussed in detail.

The emplacement of alkali feldspar microgranites were structurally controlled by a system of faults and joints. Rock/fluid interaction displaying a petrographical zonal pattern, with lower unaltered miarolitic pink alkali-feldspar granite zone, a middle zinwaldite amazonitized (microclinized) granite zone and a roof zone of zinwaldite albitized granite, where both amazonitization and albitization took place along fractures and joints of the stock as banded occurrence (Fig.2) ,(Abdalla et al., 1996).

Amazonitization zone is characterized by the development of highly to fully ordered green microcline (imparting to rock a pale to deep green color), zinwaldite and spessartine garnets replacing pre-existing minerals (Fig.3). The amazonite (in thin section), exhibits the cross-hatched twinning and the percline twins of the replaced albite (Fig.4A). Magmatic quartz can be texturally distinguished by its subhedral shapes, corrosion features, whereas hydrothermal quartz shows irregular shapes, fills interstices and is intergrown with microcline and perthitic orthoclase (Fig. 4B), generating incipient granophyric textures. Accessory minerals are fluorite, zircon (Fig. 5), columbite, autonite (Fig.6), ilmenite, thorite and acicular uranophane. Abundant degassing breccias are observed and composed mainly of fragmented euhedral to subhedral violet and colorless fluorite crystals embedded in a fine-grained matrix of felsic minerals (Fig. 7 and 8).

Albitization zone is characterized by abundant subsolidus clusters of fine-grained albites replacing early formed microcline along cleavage and twinning planes (Fig. 9), with development of zinwaldite and spessartine in the same time. Accessory minerals as the same in amazonitization zone and increase in abundance. Many quartz veins and quartz breccia traverse the granitic mass and stike E-

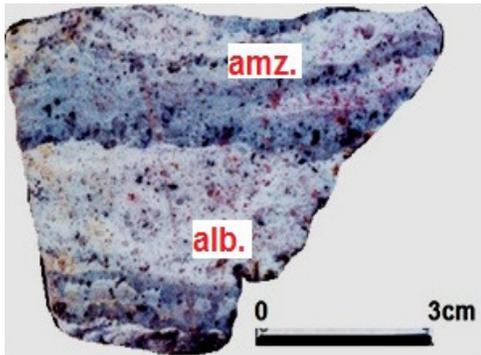


Fig. 2: A polished slab showing banded amazonitized (amz.) and albitized (alb.) in alkali feldspar microgranite



Fig. 3: A photomicrograph showing development of zinnwaldite (Zw.) replacing pre-existing quartz, XPL

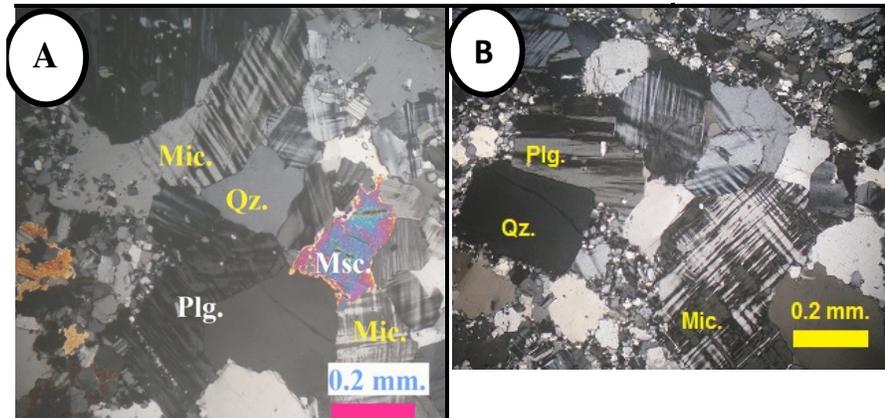


Fig. 4. A photomicrograph showing (A) a cross hatched microcline crystals (Mic.) replacing plagioclase (Plg.), (B) secondary quartz blebs intergrown with microcline crystals, XPL



Fig. 5: Photomicrograph showing euhedral crystal of metamict zircon within amazonitized granite, XPL

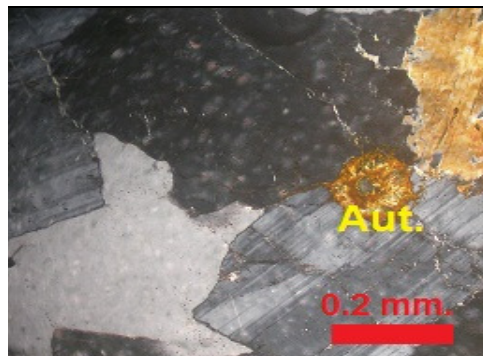


Fig. 6: Photomicrographic showing an autunite crystal rimmed with iron oxides engulfed within plagioclase crystal, XPL

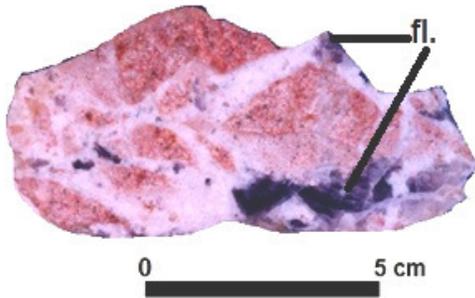


Fig. 7: A polished slab showing a degassing breccias where euhedral fluorite crystals (fl.) embedded in a fine grained felsic matrix

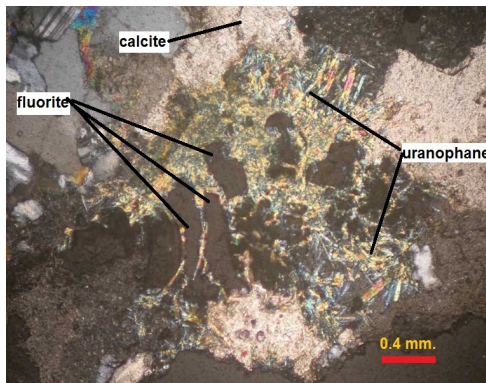


Fig. 8: Acicular crystals of uranophane intergrown with fine calcite crystals and fluorite along joint planes, XPL

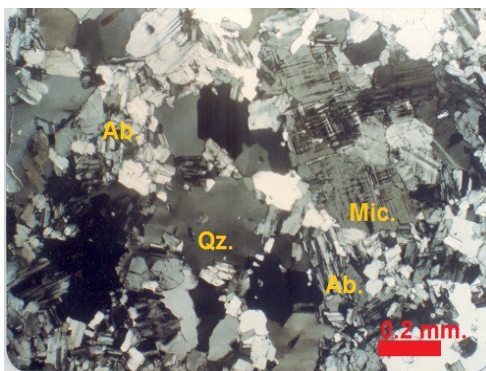


Fig. 9: Photomicrograph showing the development of subsolidus albite (Ab.) laths which attack the preexisting K-feldspar (Mic.), XPL

W direction.

Although albitization occurs on a regional scale, the mechanism takes place on the scale of individual mineral grains. Albitization is commonly associated with scapolitization and the formation of ore deposits (Ettner et al., 1993; Munz et al., 1994; Oliver et al., 1994; Schandl et al., 1994; Frietsch et al., 1997; Mark and Foster, 2000). Understanding the process of albitization is an essential component of developing a coherent model for such mineralization. Regional-scale albitization involves the transport of solution over long distances (kilometers) and requires a transport mechanism by which fluid can pass through originally low-permeability rocks. The replacement of plagioclase and alkali feldspars by albite has been documented by Saigal et al., (1988), Petersson and Eliasson (1997), Lee and Parsons (1997) and Leichmann et al., (2003) and others. In a more general sense, the replacement of one feldspar by another is commonly associated with fluid-rock interaction and metasomatism. Harlov et al., (1998) and Putnis et al., (2007a) have demonstrated the metasomatic replacement of plagioclase by K-feldspar. A characteristic feature of replaced feldspars is the development of turbidity due to porosity formation, as described by Walker et al., (1995). Where the interacting fluid or the parent feldspar contains Fe, the replacement mechanism can result in the precipitation of hematite within the pores, producing red-clouded feldspars. It has been proposed that porosity generation is an integral feature of the interface-coupled dissolution-precipitation mechanism of re-equilibrating minerals in the presence of a fluid phase (Putnis, 2002; Putnis et al., 2005; 2007b, Putnis and Putnis, 2007).

In places with Na-metasomatism being overwhelming, the albitite rock has a patchy and erratic distribution of limited areal extent. Albitite is white, fine-grained, composing up of > 90% albite with an average grain size < 0.2 mm, where small relics of microcline

and corroded quartz grains are observed to be replaced by fine albite laths (Fig.10 a and b), also bladdered columbite crystals embedded within fine grained albite laths are observed (Fig.11). The alteration sequence continued with Fe (hematitization) and Mn-oxide alteration along later fractures and joints as local impregnations.

Field observations and microscopic examinations revealed two modes of occurrences for uranium mineralization: (1) disseminated mineralization as acicular crystals of uranophane in the albitized granite (Fig.12). (2) fracture-filling in the amazonitized and albitized granites. The fracture-filling uranophane occurs as crystalline aggregates

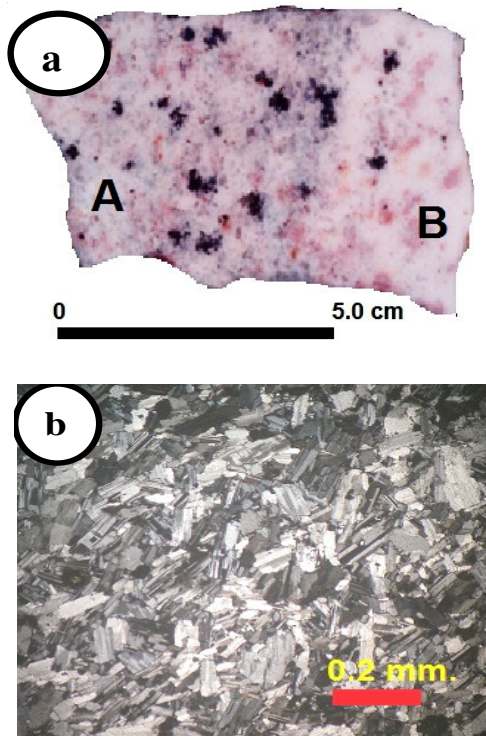


Fig. 10: (a) A polished slab showing a strongly albitized alk. Feldspar (A portion), transformed into albitite (B portion). (b) A photomicrograph showing albitite rock when albitization becomes overwhelming. XPL

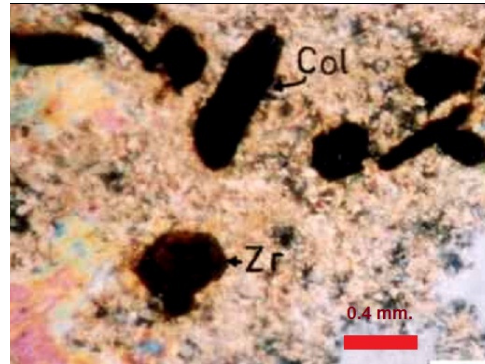


Fig. 11: Photomicrograph showing a bladdered columbite (Col.) crystals, metamict zircon (Zr.) embedded within fine grained matrix in albitized granite. XPL

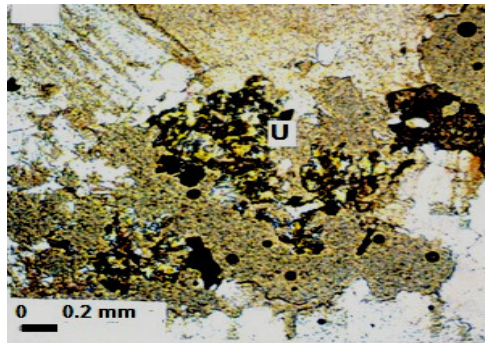


Fig. 12: Acicular crystals of uranophane disseminated within albitized granite, PPL

intergrown with fine calcite crystals during the opening of the fractures and loss of volatiles (particularly CO_2) (Figs. 8 and 13). The fracture-filling uranophane is associated with late-stage of Fe and Mn-oxide alteration.

MODE OF OCCURRENCE

The evolved nature of the alkali-feldspar granite suggests melting of older anhydrous crust by ascending mafic magma underplating the base of extended stabilized late Precambrian crust of the Nubian Shield. The extraction of a monzogranite protolith which was emplaced during the post-orogenic phase led to a residual melt depleted in Ca, Ba, Sr, and enriched in Zn, Pb, Ga, Li, Rb, high charge

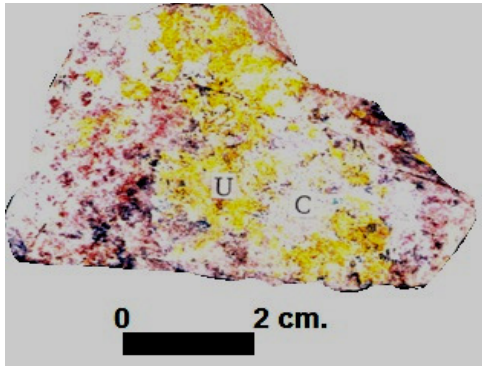


Fig. 13: A close view of uranophane (U) and calcite (C) along microfracture surface, (hand specimen)

cations and an anhydrous volatile phase (e.g., F, Cl and CO_2), (Abdalla, 1996). The presence of F, Cl, CO_2 and the alkalis Na, K, Li and Rb in the melt allowed stable complexing of the high charge elements (Abdalla, Op.Cit. and Hildreth, 1981). The elements (Na, Li, Rb, and U) and (Zr., Nb, and Y) are efficiently stabilized by F- and Cl-rich residual fluid phase, respectively (Hildreth, 1981). Extension of the continental crust permitted this evolved and less dense magma to rise and produce shallow magma chambers, where it solidified into alkali-feldspar granite cupola co-existing with an exsolved supercritical fluid. This fluid phase was initially confined to grain boundaries, microstructures, and vugs (Pollard and Taylor, 1986). The fluid phase was further separated into a highly mobile volatile phase and a low density aqueous fluid. Textural characteristics e.g., miarolitic cavities, degassing breccias and the pegmatite nests are good evidence for early separation of a volatile phase.

According to the available experimental data, the early high temperature reactions proceeded through K-metasomatism where K^+ , Rb^+ and Pb^{2+} in the fluid replaced Na and Ca of early existing feldspars. The high contents of Rb and Pb of the amazonitized microgranites are found to be incorporated within the K-feldspar

(green amazonite) structure (Abdalla et al., 1996). The released Na and Ca during the K-metasomatism were stabilized in the albite with veinlet fluorite in the roof zone of albitization process. These reactions may proceed towards increasing Al_2O_3 , and Na_2O with contemporaneous desilicification when the albitization becomes extensively overwhelming. The gross enrichment of the radioactive minerals towards the roof Na-rich zones indicates that these elements have been stabilized by a highly mobile diffusing volatile phase (e.g., F, Cl, Na, K, Rb and Li) during their transportation. The decreasing temperature, salinity, the loss of CO_2 (and other volatiles) and the increasing pH are considered the essential factors for radioactive mineralization at more evolved phases of alkali feldspar microgranites (Abdalla et al., 1996).

RESULTS OF SPECTROMETRY

A detailed survey on the different rock varieties is done (with special interest for alteration zones and contacts between alkali feldspar microgranite and Dokhan volcanics) to locate anomalous zones of gamma-radiations and to determine the lithological characteristic of these zones. By the means of the gamma-ray spectrometry, it is possible to determine the individual concentrations of the three naturally occurring radioelements (K%, eU and eTh) in different rock varieties. The results of spectrometric survey expressed in ppm for eU, eTh and % for K comprising about 415 stations for the three rock varieties (Um Dobr Dokhan volcanics, monzogranites and alkali feldspar microgranites) as shown in Table(1), and graphically represented by frequency histograms and binary diagrams (Figs. 14 &15).

Table.1 illustrates the minimum, the maximum and the average values for each rock unit. From the table, we can notice that eU in Dokhan volcanics is in the range of 2 to 42 ppm with an average value of 10 ppm and in monzogranites, it varies from 3 to 13 ppm with an average of 7 ppm while in alkali

Table 1: Minimum, maximum, average readings of K %, eU, eTh (ppm) and (Bq/kg), in addition hazard indices

Rock type	No. of readings	K%	eU (ppm)	eTh (ppm)	K (Bq/kg)	eU (Bq/kg)	eTh (Bq/kg)	Dose	Eff. Dose	Ra _{eq}	H _{ex}	H _{in}	I _γ
Dokhan Volcanics	Min.	1.1	2	5	344.3	24.8	20.2	38.02	0.05	80.14	0.22	0.28	0.60
	56 Max.	5.8	42	51	1815.4	520.8	206.04	440.76	0.54	954.8	2.58	3.99	6.74
	Av.	3.1	10	18	970.3	124	72.72	141.67	0.17	302.5	0.82	1.15	2.20
Monzo granite	Min.	1.7	3	11	532.1	37.2	44.44	66.22	0.08	141.6	0.38	0.48	1.05
	120 Max.	5	13	47	1565	161.2	189.88	254.42	0.31	552.8	1.49	1.93	4.02
	Av.	3.5	7	26	1095.5	86.8	105.04	149.23	0.18	321.1	0.87	1.10	2.36
Alkali feldspar granite	Min.	1.2	3	14	375.6	37.2	56.56	67.01	0.08	146.9	0.40	0.50	1.06
	239 Max.	6.3	283	83	1971.9	3509.2	335.32	1906	2.34	414.0	11.2	20.7	28.0
	Av.	3.8	30	46	1189.4	372	185.84	333.71	0.41	724	1.97	2.98	5.13
International average								57	0.48	370	1	1	0.5

feldspar microgranites eU contents vary from 3 to 282 ppm with an average value of 30 ppm. The (eTh) contents in Dokhan volcanics ranges from 5 to 51 ppm with an average 18 ppm, in monzogranites their contents were in the range of 11 to 47 ppm with an average value of 27 ppm where it ranges from 14 to 83 ppm with an average 46 ppm in alkali feldspar granite. It is clear that alkali feldspar granites are more enriched in U content in comparison with the other two varieties due to metasomatic alterations which proved petrographically. Also, a slightly high eU contents in Dokhan volcanics may be attributed to the excess concentration of uranium bearing refractory minerals.

To evaluate the concentrations of eU and eTh in different varieties using frequency histograms (Fig.14.), which can give us an idea about the limit of concentration predominant in each variety. From this table, we can recognize that the majority of readings for eU concentration in the range between 4 and 12 ppm in volcanics, between 3-10 ppm for monzogranites and between 30-60 ppm for alkali feldspar microgranite. Also, eTh may range between 6 and 30 ppm in volcanics, between 12 and 40 ppm in monzogranites and ranges between 15 and 85 ppm in alkali feldspar mi-

crogranite.

Using binary diagrams to compare between the eU and eTh content in the three varieties (Fig.15) indicate weakly positive relation between eU vs. eTh in Dokhan volcanics and monzogranites, while in alkali feldspar granite two increasing trend groups clears two sets of concentrations trends. The relationship between eTh vs. eU/eTh shows slightly increasing trend in Dokhan volcanics due to excess of U, while monzogranites and alkali feldspar granite declares decreasing trend. The relationship between eU vs. eU/eTh in Dokhan volcanics and monzogranites shows increasing trends and in alkali feldspar granites show strongly increasing trend due to more enrichment in U as a result of presence of U minerals such as uranophane and autonite as well as secondary minerals bearing radioactive elements (U, Th) such as columbite, zircon, monazite, xenotime and fluorite.

EQUILIBRIUM AND DISEQUILIBRIUM

In closed systems, the radioactive decay of U and Th reaches a state of equilibrium when the production rate of any intermediate daughter in the decay series equals its decay rate. According to Reeves and Brooks,

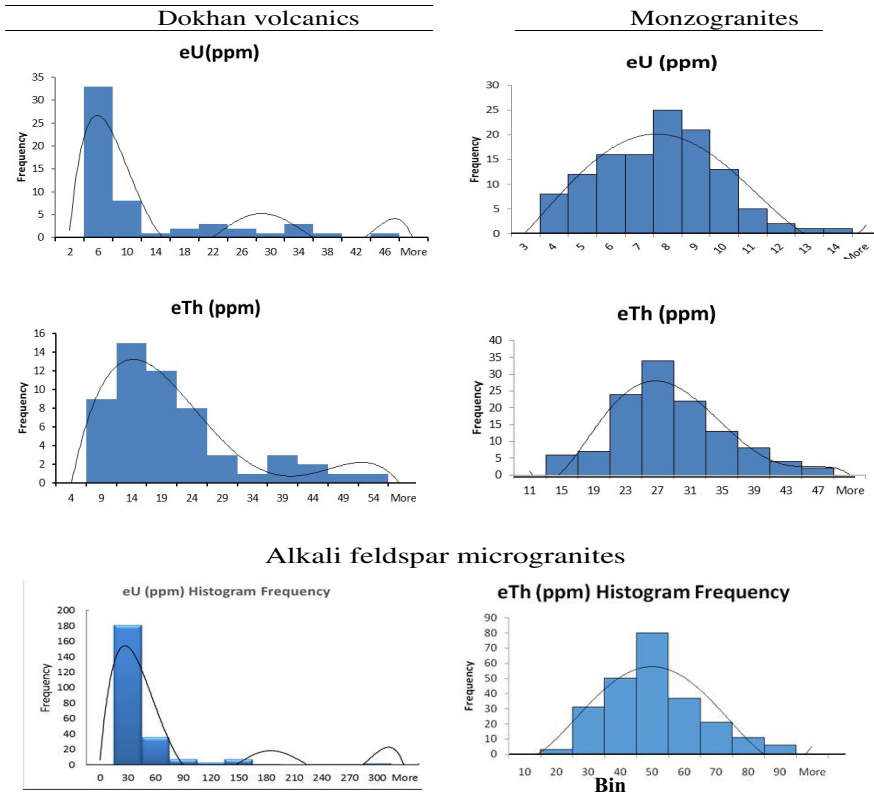


Fig. 14: A comparison between eU and eTh content (in ppm) in both Dokhan volcanics, monzogranites and alkali feldspar microgranites using a histogram frequency

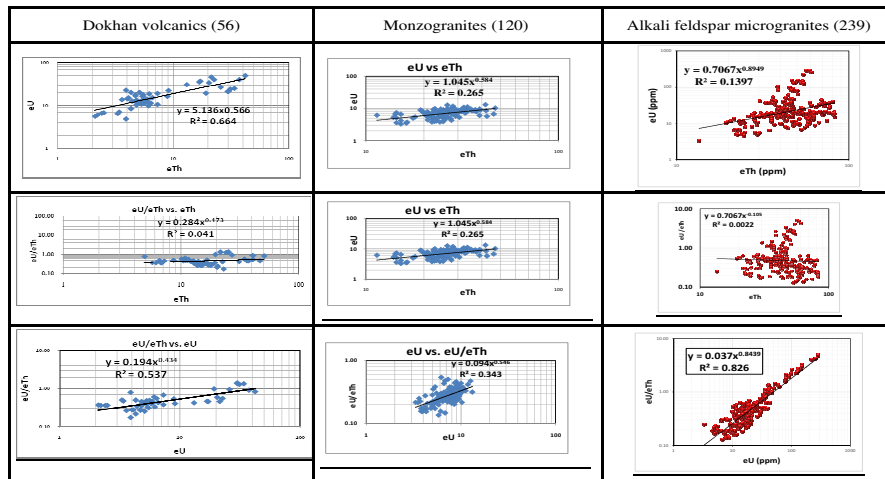


Fig.15: A binary digrams using eTh vs. eU, eTh vs. eU/eTh and eU vs. eU/eTh to compare between different varieties in the study area.

(1978), uranium (^{238}U series) attains the equilibrium state in nearly 1.5 M.a. Leaching, mobility and redistribution of uranium are affected by hydrothermal solutions and/or supergene fluids, which cause disequilibria in the radioactive decay series in the U bearing rocks. In nature, the equilibrium state is controlled by different geologic processes such as weathering, alteration, groundwater and meteoric water migration, circulating fluids through fractures and fault planes and loss of radon gas as one of uranium daughters. These processes may cause disturbance in the equilibrium state by addition or removal of uranium and hence disequilibrium arises. The results of U content measured chemically (U_{ch}) compared with eU values in addition with the ratio between them (D-factor, after Hansink, 1976) is listed in (Table.2). If the D-factor was more or less than unity, it indicates addition or removal of uranium respectively (Hansink, 1976 and Stuckless et al., 1984). It is clear that the chemical uranium(U_{ch}) is greater than the radiometric uranium which means disequilibrium state. This explained by plotting eU (radiometrically measured) against U_{ch} . The Figure (16) shows that all samples are plotted above the line $U_{ch}/eU=1$ due to addition of uranium (recent uranium) reflecting disequilibrium state.

ASSESSMENT OF DOSE

Absorbed Dose Rate in Air (D)

Concentrations of ^{40}K , ^{238}U and ^{232}Th are usually given in equivalent ground concentrations: K (%), eU (ppm) and eTh (ppm), respectively. The specific parent activity of a sample containing 1 ppm of ^{232}Th and 1 ppm of natural U is 4.08 and 13.0 Bq/kg^{-1} , respectively. For natural potassium, a concentration of 1% by weight of sample corresponds to a ^{40}K -specific activity of 317 Bq/kg^{-1} .

The absorbed gamma dose rates in air at 1m above the ground surface for the uniform distribution of radionuclides (^{226}Ra , ^{232}Th and ^{40}K) were calculated by using Eq.(1) on the

Table 2: Radimetrically measured uranium (eU), chemically measured (U) and eU/U ratio for selected samples of altered alkali feldspar microgranite

Sample No.	spectrometric measurements (eUppm)	Chemical analyses (U_{ch}) (ppm)	U_{ch}/eU
1	45	48	1.07
2	48	53	1.10
3	41	56	1.37
4	44	52	1.18
5	52	57	1.10
6	53	63	1.19
7	50	60	1.20
8	60	65	1.08
9	61	64	1.05
10	63	69	1.10
11	57	70	1.23
12	65	72	1.11
13	72	82	1.14
14	88	94	1.07
15	118	163	1.38
16	115	123	1.07
17	154	178	1.16
18	25	36	1.44
19	27	35	1.30
20	32	36	1.13
21	30	40	1.33
22	41	50	1.22

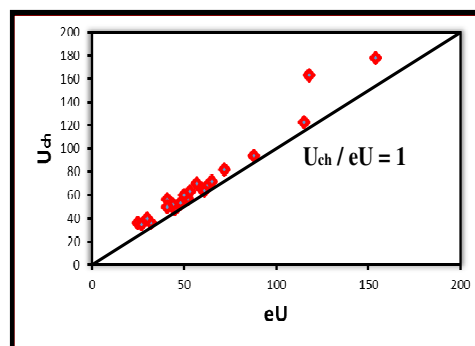


Fig.16: Binary diagram showing equivalent uranium (eU) vs. chemically measured (cU)

basis of guide lines provided by UNSCEAR (2000) (Fg ün et al., 2007).

$$D (\text{nGy h}^{-1}) = 0.462A_{\text{Ra or U}} + 0.604A_{\text{Th}} + 0.0417A_{\text{K}} \quad (1)$$

Where $A_{\text{Ra or U}}$, A_{Th} and A_{K} are the average specific activities of ^{226}Ra or U, ^{232}Th and ^{40}K in Bq/kg , respectively.

Annual Effective Dose Equivalent (AEDE)

The annual effective dose equivalent (AEDE) was calculated from the absorbed dose by applying the dose conversion factor of 0.7 Sv/Gy and the outdoor occupancy factor of 0.2 (UNSCEAR, 2000, Anjos et al., 2005, řg ün et al., 2007).

Radium Equivalent Activity (Ra_{eq})

The radium equivalent activity for the samples was calculated. The exposure to radiation (Tufail et al., 1992) can be defined in terms of the radium equivalent activity (Ra_{eq}), which can be expressed by the following equation:

$$Ra_{eq} = A_{Ra\ or\ U} + 10/7A_{Th} + 10/130A_K \quad (2)$$

Where $A_{Ra\ or\ U}$, A_{Th} and A_K are the specific activities of Ra or U, Th and K, respectively, in Bq/kg.

External and Internal Hazard Index (H_{ex} and H_{in})

To limit the annual external gamma-ray dose (Saito and Jacob, 1995; Saito et al., 1998; UNSCEAR, 2000) to 1.5 Gy for the samples under investigation, the external hazard index (H_{ex}) is given by the following equation:

$$H_{ex} = A_{Ra\ or\ U}/370 + A_{Th}/259 + A_K/4810 \quad (3)$$

The internal exposure to ^{222}Rn and its radioactive progeny is controlled by the internal hazard index (H_{in}), which is given by Nada (2003):

$$H_{in} = A_{Ra\ or\ U}/185 + A_{Th}/259 + A_K/4810 \quad (4)$$

These indices must be less than unity in order to keep the radiation hazard insignificant (Lakehal et al., 2010; Baykara et al., 2010).

Activity Concentration Index (I_γ)

Another radiation hazard index called the representative level index, I_γ , is defined as follows (NEA-OECD, 1979):

$$I_\gamma = A_{Ra\ or\ U}/150 + A_{Th}/100 + A_K/1500 \quad (5)$$

where $A_{Ra\ or\ U}$, A_{Th} and A_K are the activity concentrations of ^{226}Ra or ^{238}U , ^{232}Th and ^{40}K , respectively in Bq/kg

(Abbady et al., 2005). The safety value for this index is ≤ 1 (El Galy et al., 2008; El Aassy et al., 2012, Sadek et al., 2014).

Environmental Impacts

The minimum, maximum and average absorbed γ - dose rate (D) values for the studied rocks are shown in Table (1). The values obtained in Dokhan volcanic samples are ranged between 38.02 and 440.76 nGyh⁻¹ with an average 141.67 nGyh⁻¹, for monzogranites, these values varied from 66.22 to 254.42 nGyh⁻¹ with an average value of 149.23 nGyh⁻¹ and for alkali feldspar granites, the absorbed γ -dose rate (D) ranged from 67.01 to 1906.01 nGyh⁻¹ with 331.71 nGyh⁻¹ as an average. These estimated values of absorbed γ - dose rate in the studied Dokhan volcanic, monzo- and alkali feldspar granite samples are comparably higher than the world average value 57 nGyh⁻¹ (Tzortzis et al., 2003, Abbady et al., 2005, Sadek et al., 2014).

Furthermore, the average values of annual effective dose for all the studied rocks were also listed. The values obtained varied between 0.05 and 0.84 mSvy⁻¹ for Dokhan volcanics, 0.08 and 0.31 mSvy⁻¹ for monzogranites and 0.08 and 2.34 mSvy⁻¹ for alkali feldspar granites. The mean value (0.17, 0.18 and 0.41 for Dokhan volcanics, monzo- and alkali feldspar granites, respectively) found to be less than 0.48 mSvy⁻¹ [recommended by UNSCEAR (2000) as the worldwide average of the annual effective dose.

The radium equivalent activity Ra_{eq} range for Dokhan volcanics samples were between 80.14 and 954.79 Bq/Kg-1 with 302.52, Bq/Kg⁻¹ as a mean value, 141.62 and 552.84 Bq/Kg⁻¹ with 321.13 Bq/Kg⁻¹ as an average for monzogranite and from 146.89 to 4139.91 Bq/Kg⁻¹ with an average value of 728.98 Bq/Kg⁻¹. The values radium equivalent activity (Ra_{eq}) are lower than the recommended maximum value of 370 Bq/ kg⁻¹ for Dokhan volcanics and monzogranite whereas alkali feldspar granites Ra_{eq} is higher than the maximum permitted value due to their high contents of

radionuclides.

The values of external and internal hazard indices (H_{ex} and H_{in}) for Dokhan volcanics range between 0.22 and 2.58 and 0.28 to 3.99, respectively, 0.38 and 1.49 and 0.48 and 1.93, respectively, for monzogranites and between 0.40 and 11.19 and 0.50 and 20.67, respectively, for alkali feldspar granites. Average of external and internal hazard indices are higher than unity for studied alkali feldspar granites indicating that these granites cannot be used as building and interior decorative material of dwelling.

The gamma activity index ($I\gamma$) used to assess safety requirement for building materials were evaluated and presented in Table (1). The average values of gamma activity index ($I\gamma$) for Dokhan volcanics, monzo- and alkali feldspar granites were 2.2, 2.36 and 5.13, respectively. The obtained values of gamma activity indices in the studied rocks were higher dose criterion (0.3mSv/y) and corresponds to an activity concentration index of $2 \leq I\gamma \leq 6$ proposed by EC (1999) for materials used in bulk construction.

CONCLUSIONS

The geologic setting, textural, and petrographical characteristics indicate that the zonal pattern of Um Ara alkali feldspar granite has been developed as the result of subsolidus reactions of an exsolved post-magmatic fluids with the already consolidated alkali-feldspar microgranite. The gross enrichment of the radioactive elements (U and Th) towards the roof Na-rich zone indicates that these elements have been stabilized by a highly mobile diffusing volatile phase (i.e., F, Cl, Na, K, Rb and Li) during their transportation. However, the decreasing temperature and salinity and the loss of CO₂ (and the other volatiles) and increasing pH are considered the essential factors for uranium localization at Um Ara alkali feldspar microgranite. Field observations and microscopic examinations revealed two modes of occurrences for uranium mineraliza-

tion: disseminated mineralization as acicular crystals in the albitized granite, and fracture-filling in the amazonitized and albitized granites. The fracture-filling uranophane occurs as crystalline aggregates intergrown with fine calcite crystals during the opening of the fractures and loss of volatiles (particularly CO₂). The fracture-filling uranophane is associated with late-stage Fe and Mn-oxide alteration. The results of spectrometric survey revealed that the alkali feldspar granite are more enriched in U content (eU ranges between 13-84 ppm. With average 46 ppm) in comparison with the other two varieties (Dokhan volcanics and monzogranite) due to metasomatic alterations, while a slightly high eU contents in Dokhan volcanics may attributed to the excess concentration of uranium bearing refractory minerals (e.g, zircon).

The relationship between eU vs. eU/eTh declares weakly increasing trends in Dokhan volcanics and decreasing trends in monzogranites but shows strongly increasing trends in alkali feldspar granites due to more enrichment in U as a result of presence of U minerals such as uranophane and autonite as well as U and Th bearing radioactive minerals such as columbite, zircon, monazite, xenotime and fluorite.

Gamma-radiation dose rate and annual effective dose equivalents in mSv/y, Radium equivalent activity, external (H_{ex}) and internal hazard index (H_{in}) and gamma activity index ($I\gamma$) for all investigated samples were calculated to assess the potential radiation hazard for people living in dwellings made of the studied granites. Alkali feldspar granite activities would suggest that caution must be taken when using granites as building materials because they have radioactivity above the proposed acceptable level.

REFERENCES

- Abbady, A.G.E.; Uosif, M.A.M., and El-Taher, A., 2005. Natural radioactivity and dose assessment for phosphate rocks from Wadi El-Mashash and El-Mahamid Mines, Egypt. *J. Envi-*

- ron. *Radioact.*, 84, 65–78.
- Abd El-Naby, H.H., 2009. High and low temperature alteration of uranium and thorium minerals, Um Ara granites, south Eastern Desert, Egypt. *Ore Geo. Rev.*, 35, 436–446.
- Abdalla, H.M., 1996. Geochemical and mineralogical studies at Um Ara rare metals prospect, Southeastern Desert, Egypt. Unpub. Ph. D. Thesis, Hokkaido University, Sapporo, 178 p.
- Abdalla, H.M.; Ishihara, S.; Matsueda, H., and Abdel-Monem, A.A., 1996. On the albite-enriched granitoids at Um Ara area, Southeastern Desert, Egypt: I. Geochemical, ore potentiality and fluid inclusion studies. *J. Geochemical Exploration*, 57, 127–138.
- Abdel Meguid, A.A., 1986. Geologic and radiometric studies of uraniumiferous granite in Um Ara-Um Shilman area, south Eastern Desert, Egypt. Ph.D. Thesis, Suez Canal Univ., Egypt, 241p.
- Abdel-Meguid, A.A.; Ibrahim, T.M.M., and Elawadi, E.A., 2007. Factors Controlling Uranium Mineralization. In: Um Ara Granite, South Eastern Desert, Egypt. SGA_A289.
- Abu Dief, A., 1985. Geology of uranium mineralization in Missikat, Qena-Safaga road, Eastern Desert, Egypt. M.Sc. Thesis, Assiut Univ., Egypt, 242p.
- Abu Dief, A. 1992. The relation between the uranium mineralization and tectonics in some Pan-African granites, west of Safaga, Eastern Desert, Egypt. Ph.D. Thesis, Assiut Univ., Egypt, 218 p.
- Abu-Zeid, M.M., 1995. Relation between surface and subsurface uranium mineralization and structural features of Gabal Qattar, Northeastern Desert, Egypt. M.Sc. Thesis, Ain Shams Univ., Cairo, Egypt, 209p
- Anjos, R.; Veiga, R.; Soares, T.; Santos, A.; Aguiar, J.; Frascac, M.; Brage, J.; Uzeda, D.; Mangia, L.; Facure, A.; Mosquera, B.; Carvalho, C., and Gomes, P., 2005. Natural radionuclide distribution in Brazilian commercial granites. *Radiat. Meas.*, 39, 245–253.
- Awadallah, E., 1999. Mineralogy and geochemical characteristics of uranium-bearing granites, North Um Ara, South Eastern Desert with emphasis on uranium extraction, Ph.D. Thesis, Ain Shams Univ.
- Bakhit, F.S., 1978. Geology and radioactive mineralization of Gabal El Missikat area, Eastern Desert, Egypt, Ph. D. Thesis, Ain Shams Univ., Cairo, Egypt, 282p.
- Baykara, O.; Karatepe, S., and Dođru, M., 2010. Assessments of natural radioactivity and radiological hazards in construction materials used in Elazig, Turkey. Technical Report. *Radiat. Meas.* doi: 10.1016 / J. Radmeas. 2010.08.010. (In press).
- Dahlkamp, F.J., 1978. Classification of uranium deposits. *Mineral Deposita*, 13, 83-100.
- Dahlkamp, F.J., 1980. Typology and geographic/geotectonic distribution of uranium deposits. In: P.F. Buroillet and V. Ziegler (Eds.). 26th inter. Geol. congress, Collogium C-z Energy Resources. French Institute of Petroleum, Paris.
- El-Aassy, I.E.; Afaf, A.; Nada, El-Galy, M.M.; El-Feky, M.G.; Abdel Maksoud, T.M.; Talaat, Sh.M., and Ibrahim, E.M., 2012. Behavior and environmental impacts of radionuclides during the hydrometallurgy of calcareous and argillaceous rocks, Southwestern Sinai, Egypt. *Applied Radiation and Isotopes*, 70, 1024–1033.
- El-Galy, M.M.; El-Mezayen, A.M.; Said, A.F.; El Mowafy, A.A., and Mohamed, M.S., 2008. Distribution and environmental impacts of some radionuclides in sedimentary rocks at Wadi Naseib area, Southwest Sinai, Egypt. *J. Environ. Radioact.*, 99, 1075–1082.
- El-Kassas, I.A. 1974. Radioactivity and geology of Wadi Atalla area, Eastern Desert of Egypt. Ph.D. Thesis, Fac. Sci., Ain Shams Univ., Cairo, Egypt, 502 p.
- El-Shazly, E.M., 1964. On the Classification of the Precambrian and Other Rocks of Magmatic

- Affiliation in Egypt. XXII Inter. XXII Inter. Geol. Congr. Proc. Sect. 10, India, 88–101.
- Ettner, D.C.; Bjorlykke, A., and Andersen, T., 1993. Fluid evolution and Au–Cu genesis along a shear zone: a regional fluid inclusion study of shear zone-hosted alteration and gold and copper mineralization in the Kautokeino greenstone belt, Finnmark, Norway. *J. Geochem. Explor.*, 49, 233-267.
- European Commission, (EC), 1999. Radiation Protection 112-radiological protection principles concerning the natural radioactivity of building materials Directorate- General Environment. Nuclear safety and civil Protection.
- Frietsch, R.; TUISKU, P.; Martinso, N. O., and Perdahl, J.A., 1997. Early Proterozoic Cu–(Au) and Fe ore deposits associated with regional Na–Cl metasomatism in northern Fennoscandia. *Ore Geol. Rev.*, 12, 1-34.
- Hansink, J.D., 1976. Equilibrium analyses of sandstone roll front uranium deposits. Inter. Atomic Energy Agency, Vienna, 683-693.
- Harlov, D.E.; Hansen, E.C., and Bigle R, C., 1998. Petrological evidence for K-feldspar metasomatism in granulite facies rocks. *Chem. Geol.*, 151, 373-386.
- Hildreth, W., 1981. Gradients in silicic magma Chambers: Implications for lithospheric magmatism. *J. Geophys. Res.* X6 (8-II), 10153-10192.
- Hussein, H.A., 1987. Geochemistry of granitic rocks and uranium mineralization in El Missikat-El Aradiya area, SW Safaga, Eastern Desert, Egypt. Ph. D. Thesis Cairo Univ., Egypt, 262p.
- Ibrahim, M.E.; Zalata, A.A.; Assaf, H.S.; Ibrahim, I.H., and Rashed, M.A., 2005. El Sella Shear Zone, South Eastern Desert, Egypt. Example of Vein-type Uranium Deposit. 9th Inter. Mining, Petroleum, and Metallurgical Engering Conf., Mining, 41–55.
- Ibrahim, M.E., 1994. Geochemistry and extraction of uranium from the uraniferous granite of Um Ara, Southeastern Desert. M.Sc. Thesis, Cairo Univ., 152p.
- Ibrahim, M.E., 1986. Geologic and radiometric studies on Um Ara granite pluton, south east Aswan, Egypt. M.Sc. Thesis, Monsoura Univ., Egypt, 177p.
- Jiashu, R., and Zehong, H., 1982. Forms of Uranium occurrence and its distribution in uraniferous granites. In: *Geology of Granites and their Metallogenic Relations*. Sciences Press, Beijing, 621–635.
- Lakehal, Ch.; Ramdhane, M., and Boucenna, A., 2010. Natural radionuclide concentrations in two phosphate ores of East Algeria. *J. Environ. Radioact.*, 101, 377–379.
- Lee, M.R., and Parsons, I., 1997. Dislocation formation and albitization in alkali feldspars from the Shap granite. *Am. Mineral.*, 82, 557-570.
- Leichmann, J.; Broska, I., and Zachovalová, K., 2003. low-grade metamorphic alteration of feldspar minerals: a Cl study. *Terra Nova*, 15, 104-108.
- Mansour, S.E.I.; El-Afandy, A.H.; Abdalla, H.M.; Saleh, G.M.; Abd El-Naby, H.H.; Abdel Wahed, A.F.; Farag, S.A.; Assran, H.M.; Ahmed, A.A.; Rashed, M.A., and Abdel Shafy, A.M., 2000. Uranium potentiality of Um Ara area, Southeastern Desert, Egypt. Internal report, Nuclear Materials Authority, Cairo, Egypt. 132p.
- Mark, G., And Foster, D.R.W., 2000. Magmatic-hydrothermal albite–actinolite–apatite-rich rocks from the Cloncurry district, northwest Queensland, Australia. *Lithos*, 51, 223-245.
- Moussa, E.M.; Stern, R.J.; Manton, W.I., and Ali, K.A., 2007. SHRIMP zircon dating and Sm/Nd isotopic investigations of Neoproterozoic granitoids, Eastern Desert, Egypt. *Precambrian Research*, 160, 341–356.
- Munz, I.A.; Wayne, D., and Austrheim, H., 1994. Retrograde fluid infiltration in the high-grade

- Modum Complex, south Norway: evidence for age, source and REE mobility. *Contrib. Mineral. Petrol.*, 116, 32-46.
- Nada, A., 2003. Evaluation of natural radionuclides at Um-Gerifat area, Eastern Desert of Egypt. *App. Radiat. Isot.*, 58, 275-280.
- Nash, J.T.; Granger, H.C., and Adams, S.S., 1981. Geology and concept of genesis of important types of uranium deposits. *Econ. Geol.*, 75, 83-116.
- NEA-OECD, Nuclear Energy Agency, 1979. Exposure to Radiation from Natural Radioactivity in Building Materials. Report by NEA Group of Experts, OECD, Paris.
- Oliver, N.H.S., Rawling, T.J., Cartwright, I., and Pearson, P.J., 1994. High-temperature fluid-rock interaction and scapolitization in an extension-related hydrothermal system, Mary Kathleen, Australia. *J. Petrol.* 35, 1455-1491.
- Ögün, Y.; Altınsoy N. S.; Ahin, S.Y.; Güngör, Y.; Gültekin, A.H.; Karahan, G., and Karacık, Z., 2007. Natural and anthropogenic radionuclides in rocks and beach sands from Ezine region (Canakkale), Western Anatolia, Turkey. *Appl. Radiat. Isot.*, 65, 739-747.
- Petersson, J., and Eliasson, T., 1997. Mineral evolution and element mobility during episyenitization (dequartzification) and albitization in the postkinematic Bohus granite, southwest Sweden. *Lithos*, 42, 123-146.
- Pollard, P.J., and Taylor, R.G., 1986. Progressive evolution of alteration and tin mineralisation: Controls by interstitial permeability and fracture-related trapping of magmatic fluid reservoirs in tin granites. *Econ. Geol.*, 81, 1795-1800.
- Putnis, A., 2002. Mineral replacement reactions: from macroscopic observations to microscopic mechanisms. *Mineral. Mag.*, 66, 689-708.
- Putnis, A., and Putnis, C.V., 2007. The mechanism of reequilibration of solids in the presence of a fluid phase. *J. Solid State Chem.*, 180, 1783-1786.
- Putnis, A.; Hinrichs, R.; Putnis, C.V.; Gollaschindler, U., and Collins, L.G., 2007a. Hematite in porous red-clouded feldspars: evidence of large-scale crustal fluid-rock interaction. *Lithos*, 95, 10-18.
- Putnis, C.V.; Geisler, T.; Schmidbeurman N, P.; Stephan, T., and Giampaolo, C., 2007b. An experimental study of the replacement of leucite by analcime. *Am. Mineral.*, 92, 19-26.
- Putnis, C.V.; Tsukamoto, K., and Nishimura, Y., 2005. Direct observations of pseudomorphism: compositional and textural evolution at a fluid-solid interface. *Am. Mineral.*, 90, 1909-1912.
- Roz, M.E., 1994. Geology and uranium mineralization of Gabel Qattar area, Northeastern Desert, Egypt. M.Sc. Thesis, Al Azhar Univ., Cairo, Egypt, 175p.
- Sadek, A; Abbas, A.H, and El-Sherif, A.M. , 2014. Natural radioactivity measurements in local and imported commercial granites used as ornamental stones. *Nuclear Sciences Scientific J.*, In Press.
- Sadek, H.S., 1978. Relation between geology and areal radiometry of Abu Swayel area, Eastern Desert. Ph. D. Thesis, Cairo Univ., Egypt, 210p.
- Saigal, G.C.; Morad, S.; Bjorlykke, K.; Egeberg, P.K., and Agaard, P., 1988. Diagenetic albitization of detrital K-feldspar in Jurassic, Lower Cretaceous, and Tertiary clastic reservoir rocks from offshore Norway. I. Textures and origin. *J. Sed. Petrol.*, 58, 1003-1013.
- Saito, K., and Jacob, P., 1995. Gamma-ray fields in air due to sources in the ground. *Radiat Prot. Dosim.*, 58, 29-45.
- Saito, K.; Pattoussi, H., and Zankl, M., 1998. calculation of the effective dose and its variation from environmental gamma ray sources. *Health Phys*, 74, 698-706.
- Salman, A.B.; El Assy, I. E., and Shalaby, M. H., 1990. New occurrence of uranium mineralization in Gebel Gattar, northeastern desert,

- Egypt. Ann. Geol. Surv. Egypt, XVI, 31-34.
- Sayed, K.F., 1996. Geochemistry of uranium and preparation of its refined concentrates from mineralized pink granites of G. Gattar and UmAra areas, Eastern Desert, Egypt. M.Sc. Thesis, Ain Shams Univ., Egypt, 105p.
- Schandl, E.S.; Gorton, M.P., and Davis, D.W. , 1994. Albitization at 1700 ± 2 Ma in the Sudbury–Wanapitei Lake area, Ontario: implications for deep-seated alkalic magmatism in the Southern Province. Can. J. Earth Sci., 31, 597-607.
- Shalaby, M. H., 1996. Structural controls of uranium mineralization at Gabal Gattar, north Eastern Desert, Egypt. Egyptian Academy of Sciences, 46, 521–536.
- Stuckless, J.S.; Nkomo, I.T.; Wenner, D.B., and Van Trump, G., 1984. Geochemistry and uranium favourability of the postorogenic granites of the northwestern Arabian Shield. Kingdom of Saudi Arabia. In: Pan-African crustal evolution in the Arabian-Nubian Shield (Convenor: A. M. Al Shanti). Bull. Fac. Earth Sci., King Abdelaziz Univ., Jeddah, Pergamon Press, Oxford, 195-210.
- Tilsley, J.E., 1979. General discussion on the theoretical and practical aspects of uranium geology. Phil. Trans. Roy. Soc. London, A 291, 447-451.
- Tones, P.D., 1981. Uranium provinces and their time-bound characteristic mineralization. Geol. J., 22, 161-174.
- Tufail, M.; Ahmed, M.; Shaib, S.; Safdar, A.; Mirza, N.M.; Ahmed, N.; Zafar, M.S., and Zafar, F.I., 1992. Investigation of gamma-ray activity and radiological hazards of the bricks fabricated around Lahor, Pakistan. Pak. J. Sci. Ind. Res. , 34, 216-220.
- Tzortzis, M.; Tsertos, H.; Christofides, S., and Christodoulides, G., 2003. Gamma-ray measurements of naturally occurring radioactive samples from Cyprus characteristic geological rocks. Radiat. Meas., 37, 221-229.
- UNSCEAR, 2000. United Nations Scientific Committee on the effect of Atomic Radiation. Sources, effects and risk of ionizing radiation, United Nation, New York.
- Walker, F.D.L.; Lee, M.R., and Parsons, I., 1995. Micropores and micropore texture in alkali feldspars: geochemical and geophysical implications. Mineral. Mag. 59, 505-534.

بتروجرافية، قياسات إشعاع جاما ومعدل الجرعة شمال شرق منطقة أم آرا ، جنوب الصحراء الشرقية ، مصر

ناصر مصطفى مغازى

أظهرت الدراسة أن الجزء الشمالي من جرانيت الفلسبار القلي دقيق التحبب - قد تعرض لإعادة صياغة متسعة نظرا للنشاط البعد مجماتي الميتاسوماتي الذي نتج عنه تطور نطاقات الامازوناتيه والاليتيه ، والتي تظهر نوعي التحول الميتاسوماتي بنوعيه (البوتاسي والصودي) والذي أدى الى اثناء كلى لعنصرى اليورانيوم والثوريوم فى المراحل الأكثر تطورا (هذا يعنى نطاقات الألبته). يُعزى تحسن محتوى اليورانيوم فى نطاقات التحول إلى معدن اليورانوفين (بنوعيه المكتنف والمالىء للشقوق) والأوتونيت- هذا بالإضافة إلى المعادن الحاملة لليورانيوم والثوريوم مثل (الكولومبيت والزركون والمونازيت والزينوتم والفلووريت. معدل جرعة اشعاع جاما والجرعة المكافئة الفعالة السنوية مقدرة بالملى سيفرت/ سنة وكذا مكافىء الراديوم النشط ودليل المخاطر الخارجية والداخلية بالإضافة الى دليل نشاط أشعاعات جاما لكل العينات محل الدراسة تم حسابها لتقييم احتمال مخاطر الاشعاعات

على الانسان الذى يعيش فى أبنية استخدم فى بناءها الجرانيت محل هذه الدراسة. وقد وجد أن نشاط الاشعاع لصخر جرانيت الفلسبار القلى لمنطقة الدراسة يقتضى الاقتراح بأخذ الحذر عند استخدامه كمادة للبناء وذلك لأن اشعاعته فوق المستوى المسموح به عالمياً.